04-499

Infrared characterization of fine-scale variability in behavior of boreal forest fires

D.J. McRae, J-Z. Jin, S.G. Conard, A.I. Sukhinin, G.A. Ivanova, and T.W. Blake

---

D.J. McRae[1], J-Z Jin, and T.W. Blake. Natural Resources Canada, Canadian Forest Service, 1219 Queen Street East, Sault Ste. Marie, ON P6A 2E5, Canada.
S.G. Conard. USDA Forest Service, Vegetation Management and Protection Research, Rosslyn Plaza, 4-C 4th Floor, 1601 North Kent Street, Arlington, VA 22209, United States.
A.I. Sukinin and G.A. Ivanova. V.N. Sukachev Forest Institute, Siberian Branch Russian Academy of Sciences, Academgorodok, Krasnoyarsk, 660036, Russia.

[1] Corresponding author (telephone; 705-541-5539; fax: 705-541-5701; e-mail: dmcrae@nrcan.gc.ca).

Abstract: Spatial and temporal variability in forest fire behavior, caused by differences in microsites, fuel types and condition, topography, and other factors across even small areas, has been poorly characterized in most previous studies. Past characterization of forest fires, especially in boreal forest conditions, has often been limited by monitoring techniques that relied on timing systems on coarse-resolution sampling grids. We report documentation and analysis of fire behaviour for several experimental fires using a camcorder-sized infrared camera mounted in a hovering helicopter positioned over the fires. These fires were conducted as part of the Russian FIRE BEAR Project in Scotch pine (*Pinus sylvestris)* forests in central Siberia. Final results provide quantitative information on fire front location, rates of spread, temperatures, and reaction intensities (kW/m^2) observed during the fires at a resolution from 2.5 to 1 m across experimental burn plots ranging from 2.3 to 4 ha. Further postfire analysis using Geographical Information System (GIS) produced a detailed spatial and temporal quantification of fireline intensity (kW/m) across the plot area. This supports clearer assessment of relationships between fire behaviour and ecological impacts. These data permit accurate fire behavior estimates at various temporal and spatial scales rather than the previous approach of usually using just an overall plot average. Rather than just a few measurements, the sample size is now quite large, allowing for statistical analysis of fire behaviour data. Overlaying of living ground fuel types using GIS analysis allowed us to evaluate their effect on fire spread and fireline intensity.

Introduction

Rate of spread is an important forest fire behavior terminology that is used to describe the horizontal movement or spread of a fire. It can be used to describe the spread at either the head, flank, or back of a fire. For fire suppression, a means of predicting a fire's rate of spread is obviously crucial in trying to combat the fire. It's importance can be seen from the various forest fire behavior prediction systems that try to predict rates of spreads based on expected burning conditions (Forest Canada Fire Danger Group 1992, Andrew et al. 2003). Rate of spread is a vital parameter in predicting fireline intensity (Alexander 1982). Byram (1959) developed the following equation for fireline intensity:

[1] $$I = Hwr$$

where I represents fireline intensity (kW/m), H is the low heat of combustion (kJ/kg), w is the fuel consumed (kg/m^2) in the flaming combustion phase, and r is rate of spread (m/s). As an influencing factor in fire effects (e.g., carbon consumption, vegetation effects, etc.), fireline intensities, calculated from rate-of-spread estimates, are an important variable to quantify for modeling these effects.

The use of modern infrared technology for documenting fire rates of spread has recently provided researchers a unique opportunity to accurately estimate fire behavior characteristics at a variety of temporal and spatial scales during experimental fires (McRae and Jin 2004). This method contrasts with most previous research efforts that often reported only an average value

for the entire fire based on only a few observations averaged over sometimes very large experimental areas (e.g., Alexander et al. 1991; Stocks 1987, 1989) with no accompanying statistical validation to give an understanding of their reliability. The conventional (on-ground) means of documenting rate of spread relies on establishing a systematic grid sampling system over the experimental plot, usually with a coarse grid spacing ranging from 10 x 10 to 20 x 20 m on 1-ha experimental plots. The rate of spread is documented by timing when the fire reaches the different grid points, which are usually marked by a non-burnable metal pin. While timing can be done visually using a watch on low-intensity fires, timing can often only be done safely through remote techniques, such as those using buried electronic timers (Blank and Simard 1983) or thermocouples attached to dataloggers (Taylor et al. 2004) that are buried in the ground to avoid fire damage.

The problem with most on-ground rate-of-spread measurements is that they provide neither sufficient data for analysis of spatial or temporal variability in fire behavior nor data sufficient for producing reliable statistical estimates of the variability in average fire behavior. Hence, there is no sense of the reliability of these estimates. The lack of statistics on fire behavior has been a result of the lack of a suitable number of observations to provide some confidence level to the average being estimated. The danger in ignoring the range in rates of spread is that it might easily mislead inexperienced fire fighters by not giving them an indication of the range of spread rates possible resulting in major safety concerns. The severity and sizes of experimental fires and concerns for research personnel safety have made it difficult to obtain a suitable sample size that would be required for estimating reliable statistics on spread rates. The inherent variability in rates of spread, even at a stand-level, is only natural due to differences in the microsite (e.g.,

ground moisture), fuel characteristics (e.g., vegetation present and densities, presence of ladder fuels, etc.), and terrain (e.g., slope). In addition, the actual physical characteristics of the firelines can affect rates of spread (e.g., junction zone effects, where two approaching fire fronts accelerate towards each other). In addition, weather conditions can affect this variability. As an example, wind speed and direction can often change even over a small time period during a fire. Assuming all other variables are constant, the fire can speed up during wind gusts and can virtually stop when lulls in the wind occur.

Our current infrared system (McRae and Jin 2004) provides continuous documentation of the fire behavior using digital infrared images, taken from a camcorder-sized camera, while hovering in a helicopter over the fire. Because of the infrared wavelength of 7.5-13 microns, the camera can easily observe fires even through dense smoke that would normally obscure visual documentation. Combined with standard Geographical Information System (GIS) techniques, a digital analysis approach can give forest fire researchers the ability to understand what is influencing the fire behavior better (e.g., fuel types, fuel loads, slopes, and microclimatic factors). Ultimately, better fire behavior models can be developed from the data obtained from remote sensing and on-ground sampling of the experimental fire plots. Since fire behavior can be better defined spatially over the plot using infrared data (e.g., some of our spatial resolution is as high as 1 x 1-m pixel sizes for this paper), fire effects (e.g., tree mortality) can be better correlated with observed fire behavior.

The basic infrared system has already been described in an earlier paper (McRae and Jin 2004). The intent of this paper is to describe some of the inherent or fine-scale variability in fire behavior that we have observed on several experimental fires conducted in Siberia, and to

provide some examples on how this can be linked with other data for improved understanding of fire behavior and fire effects. We feel that our results clearly show the ranges and variability in spread rates and energy releases that can occur within a single fire event.

Methodology

Plot establishment

This study is part of the Russian FIRE BEAR (Fire Effects in the Boreal Eurasia Region) Project. This research study was developed to address problems associated with the management of fuels, fire, and fire regimes to enhance carbon storage and forest sustainability and to minimize negative impacts of fire on global environment, wood production, and ecosystem health (McRae et al. 2004). Our research sites are located in the Yartsevo Leshoz west of the Yenisey River ($60^{o}38'$N, $89^{o}41'$E) and the Govorkova Leshoz south of the Angara River ($58^{o}35'$N, $98^{o}55'$E), in the Krasnoyarsk Region of central Siberia. All experimental fire plots measured approximately 200 x 200 m (4 ha) at Yartsevo. Plots at Govorkova were 150 x 150 m (2.3 ha) and 175 x 175 m (3.1 ha) for Fires 5 and 6, respectively. Stands in these research areas are representative of the central taiga pine forest (Parmuzin 1985). The study sites support a dry site Scotch pine (*Pinus sylvestris)*/lichen (*Cladonia* sp.)/feather moss (*Pleurozeum schreberi*) forest type, with site quality classes IV and V (Anuchin 1982). The soils are sandy alluvial-ferrous podzols supported by small-grained carbonate-free sand. There is no underlying permafrost in these forests.

In the summer, cyclone activity grows and promotes penetration of warm air from the south. While most precipitation occurs in the summer months, drought is also common here due to dry and warm air masses coming in from central Asia, Mongolia, and the central portions of eastern Siberia. During these droughts, the forest can become highly flammable. Most large fires occur from June to early August in this part of Siberia (Valendik 1990; Valendik and Ivanova 1996).

A complete fire weather station was established and maintained once researchers arrived at the site for the season (usually for the June to July period). Daily observations of dry-bulb temperature, relative humidity, barometric pressure, 10-m open wind speed, wind direction, and precipitation were taken at 1300 hours Local Standard Time (LST) to assist in calculating different fire behavior danger rating systems. Weather data from local fire airbases was used to augment our data for the early part of the fire season prior to the operation of our on-site station.

Dead fuels were sampled using a modified line-intercept method for surface fuels, and small 20 x 20-cm plots for ground fuels (McRae et al. 2004). Living ground cover is an important fuel component for fire spread in the surface fires characteristic of this system. The living ground cover was mapped using the established 25 X 25-m sampling grids as a guide (Fig 1). These maps were used in analysis of the effects of ground cover vegetation on fire behaviour.

Burning procedures

Plots were burned under a wide range in fuel moisture and weather conditions to observe effects on fire behavior, fire severity, emissions, and other ecological factors. Fires (Fig. 2) were carried out in June and July, which corresponds to the main fire season for this region. Construction of protective firelines (primarily consisting of 30-cm plowlines), ignition, and

suppression were the responsibility of the Russian Aerial Forest Protection Service (Avialesookhrana) fire management personnel. All experimental plots were burned using line ignition along the windward side to quickly create equilibrium fire behavior that mimicked wildfires under similar burning conditions (McRae 1996). Ignition commenced in the middle of the windward plot side and was carried out by two ignition teams using Russian driptorches walking quickly to either plot corner to ensure rapid ignition of the entire side. The driptorches were also used to burn out each side as the fire spread down the plot length to ensure containment of fire within the firelines. In more severe burning conditions, the firelines were widened on critical sides with a 5-m burnout strip prior to ignition of the main fire.

The infrared system

Over the past decade, commercial infrared cameras have become readily available for wildfire behavior observation. Presently, we use a FLIR ThermaCAM PM 695 camera for our observations. This camera weighs almost 2.5 kg and uses a microbolometer sensor that eliminates the mechanical cooling system of older bulkier cameras (McRae et al. 1989). A rechargeable and changeable battery powers the camera for up to 2 hours of operating time. The camera has an array format of 320 x 240 pixels and measures in the 7.5-13 micron spectral bandwidth. It can record temperatures up to 1500^{o}C, which is well within the normal temperature range found on wildfires. This ability to record high temperatures prevents over-saturation of the image pixels by the fire's temperatures. The thermal spectral bandwidth of the camera was selected as it allows sensing of background details, which can be useful in the spatial registration of individual images. The background information is essential for understanding where the fire is

actually located within the experimental plot. Near infrared (3-5 micron spectral bandwidth) would be better theoretically in capturing truer radiant energy levels, but is not necessary for monitoring fire rates of spread. A wide-angle lens enabled us to fly lower to keep below any cloud cover, as the infrared bandwidth cannot penetrate through cloud water vapor. Camera sensors provided data within ±2% of actual temperatures with a spatial resolution of 1.3 milliradians that is equivalent to a 1.0-m pixel size when the camera is flown at an altitude of 800 m above ground level. Digital images were recorded onto a PCMCIA (flash) card at the rate of one per second. A time stamp was automatically placed on each image when it was recorded. In addition, the camera was connected to a video Walkman to record the fire continuously throughout the flight.

A Russian M-8 helicopter was used for our viewing platform, as it can hover and remain stationary over the research plot. This allowed for continuous imaging of the fire's progress, which would be difficult with a fixed-wing airplane because it cannot remain stationary. A port in the floor of the helicopter was used to monitor the fire directly by the camera. The camera was held facing directly down to avoid oblique images. The camera was hand-held to allow the camera operator to focus the camera continuously onto the fire even when the helicopter was not directly over the fire. For all of our experiments, reference fires were ignited adjacent and outside of each plot corner. These fires, fuelled by down woody forest debris, acted as hot geo-reference points (ground-control points) for the spatial registration of images later in the image processing and analysis. The exact distances and azimuth between these fires were measured using survey techniques to complete this scaling process.

Infrared image analysis

It is impossible for a helicopter to remain completely steady and in a fixed position, due to atmospheric turbulence. The result is that each image collected can be quite different from one another given the altitude and heading of the helicopter when the image was actually taken. These differences would make the spatial composite of the images impossible without having the ground control points (i.e., the hot geo-reference points) present at the plot corners.

After the spatial registration of all images, initial image processing allowed us to quickly quantify various fire behavior parameters such as firefront location times and spatial distribution of temperatures (representing the pixel's average temperature). Further image processing could be done to estimate rates of spread, reaction intensity (kW/m^2), and frontal fire intensities (kW/m). The former intensity can be calculated using direct theoretical equations (Gray 1957), while the latter intensity is obtained by combining other fuel data in the GIS analysis with rate-of-spread results. Software and procedures for processing the infrared imagery have been developed during the project. Currently, we do not need to split the images into different file extension formats as was discussed in earlier work by McRae and Jin (2004). The reason for this is that the new generation of high-resolution infrared cameras can be processed with new FLIR ThermCAM processing software that enhances the image enabling the background to be seen at the same time as the fire behavior (i.e., no pixel saturation). In addition, this can all be now done in the camera's mid-temperature range setting (500-1000^oC) rather than at the highest range setting covering up to 1500^oC, which assists in capturing background information better. To ensure that the images remain useful in the analysis, three key objectives must be always observed in completing the image processing; (1) spatial registration (scaling) of all fire images

onto a selected geo-referenced image, (2) retention of the calibrated temperature values found for each pixel on the image (i.e., no pixel saturation), and (3) temporal registration of all images using a time stamp to indicate when the individual images were taken. A temperature threshold greater than 30^{o}C was used to identify which pixels contained fire activity versus normal background information (i.e., areas not burning).

Once all the synthesized images were produced, all images from an individual fire were co-registered using information from reference points and the visible image background. If a particular hot reference point was not completely discernable, selected geo-reference points (e.g., plot corners) could be used as replacements. Pixel size was determined by counting the number of pixels between the various hot-reference points and estimating the pixel size from the surveyed ground distances between the points. We combined scaled geospatial information with time stamp data on each image to calculate and map rate of spread across each plot. Image enhancement from the FLIR ThermCAM processing software allowed us to filter out the effect of hot gases rising in the plume, which made it easier to pinpoint the exact fire front location at any time on the ground.

For additional analysis of the images, we used ArcInfo and ArcView. This allowed us to interpolate the time that the fire arrived at each pixel to produce a composite image for the entire plot with isolines placed on them to show the exact location of the firefront at any time during the fire (Fig. 3). In our presentations, we used a time interval of 60 seconds to show the fire's movement. Error in the locations of the geo-reference points on composite images generated a possible mis-registration of about 1-2 pixels on some images.

Since we were predominately dealing with surface fires, it seemed that if we were able to break down our infrared data based on the mapped living ground-cover maps that we should be able to possibly improve our averages statistically, as well as obtaining better modelling data for improving rate-of-spread estimates based on the living ground-cover being traversed. Using our living ground-cover map (Fig. 1), we accomplished this by masking all ground-cover types except for the one being analyzed using ArcView.

Rate-of-spread timers

To compare with conventional on-ground measurements of fire spread, we constructed electronic timers similar to those of Blank and Simard (1983). These timers were buried next to each sample grid pin, on a 25 x 25-m grid for Yartsevo and 20 x 20-m grid for Govorkova, to record the time when the flaming front passed each pin. The basic principle for the timer use is that 3 timer values are required as input into an algorithm developed to estimate direction and rate of spread of a fire across a triangular area (Eenigenburg 1983, 1987; Simard *et al.* 1984). Visual observations with stopwatches supplemented some of the timer data. Rates of spreads obtained using these timers provided base values for comparison to the infrared results.

Results

Fire behavior experienced

We monitored six experimental fires with the infrared camera in 2000 and 2002. The weather conditions and fire danger index values at the time of these fires are shown in Table 1. All fires

were ignited in the afternoon when daily prime burning conditions would normally exist. The Canadian Forest Fire Weather Index (FWI) System (Canadian Forest Service 1987) with 3 fuel moisture codes and 3 fire behavior indices has the ability to provide more detailed information on fire behavior potential than the simpler single fire danger index systems used in Russia (Nesterov 1949; Vonsky et al. 1975). Drought Code (DC) values of the FWI System, which is a slow-drying moisture index of the deeper organic layers found in the soil, indicated two very different types of fire seasons were experienced. Based on a logarithmic scale of drying (Van Wagner 1987), the high DC values (i.e., close to 400) for Fire 2 (Table 1) indicated a severe drought was occurring in the area that should indicate the potential for deeper burning of the organic forest floor. The Initial Spread Index (ISI), a numerical rating of the expected rate of spread, of the FWI System ranged from 3.2 to 8.5 for our fires. Such values when inputted to calculate actual rates of spread in the Canadian Forest Fire Prediction System (Forestry Canada Fire Danger Group 1992) produced values from 2.8 to 10.8 m/min for the boreal spruce fuel type (Fuel Type C-2). Of all the FBP System fuel types, this fuel type is the most similar one to the Scotch pine sites of the present study as both contain a continuous feathermoss or lichen ground cover. An extreme overall fire danger, based on the Fire Weather Index (FWI) value, was recorded for Fire 2.

Except for a portion of Fire 6 (Table 2), all fires monitored were surface fires (Fig. 2). The surface fires ranged from very low intensity (Fire 1) to very high intensity (Fire 2). Given the park-like characteristics of the forest stand and the general lack of ladder fuels, a combination of high wind along with pockets of ladder fuels (e.g. patches of sapling-size trees) are necessary for a sustainable crown fire to develop in this type of forest stand. Such fire characteristics helped

explain the dominance of surface fires in this forest type and supported estimates that during normal fire years roughly 80% of the Siberian fires may burn as surface fires (Belov 1976; Furyaev 1996; Korovin 1996). Fire 6 was our highest intensity fire at 23 824 kW/m, based on Equation 1 and the ground-installed, rate-of-spread timer values, in a small open portion of the experimental plot where a patch of young trees with an average height of 8 m had regenerated (Table 2). However, the rest of this plot burned as a surface fire due to the lack of ladder fuels.

For the surface fires that did not cause tree mortality associated with extensive crown scorching (Van Wagner 1973), rates of spreads based on the ground-installed, rate-of-spread timers ranged from 1.4 to 6.8 m/min (Table 2). However, the high-intensity surface fire that caused 100% tree mortality (Fire 2) had a rate of spread of 9.0 m/min. The section of Fire 6, which had a crowning fire in it, achieved an average rate of spread of 26.7 m/min. This faster spread rate was only possible because the crowns were exposed to higher above-surface winds. Within the stand, surface fires are shielded from the stronger ambient winds that occur in the open and tend to be much slower. All trees in the area of crowning fire were killed.

Infrared Monitoring Results

As an example of the infrared monitoring and analysis capabilities, Figure 3 shows the final rate-of-spread results for Fire 5. Based on a 1.09-m pixel size, the final map provides approximately 21 406 rate-of-spread values for this 2.3-ha plot. Actual values were displayed and analyzed using standard spreadsheet software (e.g., Microsoft Excel). Figure 4a shows the distribution of all these individual observed rates of spread. The initial impression is that the shape of the histogram is bell shaped with a positive common skew with a longer right-hand tail.

The last histogram class includes all rates-of-spread values over 30 m/min. This presents the question whether all of these high values are legitimate (see Table 3). For Fire 5, the highest calculated pixel value was 991.7 m/min. The highest calculated value was 2569 m/min for Fire 3. Such high values almost certainly result from local aberrations in steady-state fire spread, especially when compared to the average pixel value of 6.5 and 5 m/min obtained from the rate-of-spread timers on those plots. Maximum values for the other fires are found in Table 3.

The intent of this study was to focus on documenting equilibrium (steady state) fire conditions. The line ignition pattern that we employed was chosen to develop these conditions as quickly as possible. However, examination of some of the rate-of-spread maps (e.g., Fig. 3) showed higher rates of spread in some areas close to the fire perimeters. We decided to eliminate the outer 10-m perimeter from analysis of each plot to reduce the influence of edge effect (where air can be entrained into the fire around its edge). This was easily accomplished by using ArcView's masking option. There were two reasons for suspecting edge effect. The first was that the Russian fire crew in our first year of experiments (Fire 2) tried to burnout down each side of the plot as the main fire carried down the middle of the plot. However, because of communication problems the burnout crews kept ahead of the main firefront rather than trying to keep slightly behind it. As a result, the firefront looked more convex in shape (Fig.5) while viewed from above rather than concave like a naturally spreading fire. This problem was corrected in succeeding years by ensuring that the burn crews kept slightly behind the main firefront to avoid influencing it. Figure 3 shows the preferred shape of the fire front that developed in the following years using this technique.

Another problem that was apparent around the edge was indrafting into the main fire from the perimeter. This was best seen aerially a few days after Fire 2, where a green strip (i.e., indicating live trees) remained only around the plot perimeter. However, all trees within the main fire area were killed when the foliage was crown scorched (i.e., lethal temperatures above 60^{o}C were produced by the fire at crown level that killed the live foliage – see Van Wagner 1973). The reason for low mortality at the fire edge was that indrafting winds into the main convection column of the fire were strong enough to keep the height of scorching below the main crown level. Van Wagner (1973) explains in his model how in fact higher wind speeds can reduce this damage by reducing the height of crown scorch damage. By eliminating the 10-m perimeter section from our analysis, the results (Table 4) were most apparent on Fire 2 where the standard deviation was substantially reduced. This should not be surprising given the problem with the burn-out operation on Fire 2 described in the previous paragraph and its effect on the fire behavior close to the perimeter.

Another area of concern in the analysis was the high numbers of large rate-of-spread values still present within the individual plots (see Table 4) once the edge-effect values were removed (e.g., a maximum rate of spread of 2569 m/min was indicated on Fire 3 where the average plot value was only 16.9 m/min). In most cases, these values appeared to coincide with locations where an irregular firefront existed, where there was a development of fingers or a local convergence zone in the fire front. It was not entirely clear whether some of these values were indeed legitimate over the very small areas involved or whether an interpretation error had occurred due to the points and times used in the algorithm (Eenigenberg 1987) used in predicting the rate of spread. This latter error would be more likely if there was a delay in taking

consecutive images quickly (i.e., not a continuous sequence of images to show the fire spread movement adequately). This might occur if the helicopter had to reposition itself while monitoring the fire. In many cases, the camera operator just did not capture the sequence between images quickly enough in an attempt to avoid filling the PCMCIA (flash) card prematurely before the end of each fire to capture this junction-zone effect correctly, as our main objective during these burns was to capture equilibrium fire spread conditions and not short-lived extreme phenomena (such as junction zones).

Some of the high rate-of-spread values that might indicate junction zones could be eliminated quickly because of prior knowledge of the area that the effect could not have been possible because of prefire sampling. Most notable in these cases were wet depressions where high rates of spread could not have occurred. Since our main goal for fire behavior characterization was to be able to predict equilibrium rates of spread, we decided to eliminate all values more than ± two standard deviations from the mean, which left 95% of the values in the data set for analysis. Table 5 shows these results and should be considered as a good representation of the equilibrium fire spread conditions experienced during these fires.

As in most living forests, there was a diverse make-up of the living ground cover across these dry Scotch pine sites. As an example, we compared two large areas of living ground-cover on Fire 2, as they were probably affected by the same wind influences as fire spread across them over the same time period. Fire spread through the blueberry (*Vaccinium* sp.)/feathermoss/lichen ground-cover type at an average of 9.8 m/min compared to the more moist blueberry/feathermoss sites where the fire spread an average of 4.5 m/min. Comparing these values to the overall plot average of 5.6 m/min (Table 5) shows how microsites can affect rates of spread.

Using ArcView, we estimated fireline intensity (Fig. 6) by combining the rate of spread image with a spatial database on fuel consumption at each of the grid sample points. These data were contoured across the entire plot using ArcView. In addition, residence times can be determined based on the time each point remains above a threshold temperature at which flaming combustion is considered to occur. We used a threshhold pixel temperature value of 150^{o}C to indicate flaming combustion. This value is lower than typical flame temperatures, but it must be realized that we are dealing with pixel temperatures rather than actual on-ground temperatures. Pixel temperatures are lower as a result of averaging the temperature across the entire pixel. Observed temperatures may also be slightly lower due to the fact that we were dealing with surface fires burning underneath the vegetation canopy that may mask some of the radiant energy being emitted by the fires. Infrared images can be further analyzed to understand flame depth at any time during the fire along the entire fire front (Fig. 7).

Discussion

The initial capital cost of acquiring an infrared camera of the resolution needed for this type of monitoring may be high to some groups Aerial surveillance using the camera can also be high when aircrafts must be rented. However, the data resolution that is obtained offsets these disadvantages. A key aspect in spatial registering of the various images in the analysis is the use of the reference fires at the four corners of the fire plot. This does take an added effort during the fires to keep these reference fires burning hot enough on the images, especially when on-ground research personnel are involved in other duties. Error in the locations of the geo-reference points on composite images generates a possible mis-registration rate of about 1-2 pixels during the analysis depending upon pixel size. This is caused when the reference fires do not completely cover the pixel area. The result is that the analyst can locate the pixel with the reference fire in it, but not precisely where the fire is within the actual pixel. Therefore, when registering a number of geo-reference points on composite images what is being fixed is the reference pixel rather than the exact spot where the reference fire is burning. It should also be noted that the exact location of the same reference fire within a pixel can vary between images, as the camera's area of view changes with the movement of the helicopter. Therefore, any two images can have their reference fires located at different locations within each individual pixel area. In fact, registrations fires could also in some cases be shared between pixels. This mis-registration affected the estimated rate of spread, especially at low rates. This problem can also increase the density of fire isolines on the final maps (e.g., Fig. 3 and 5) when fire spread is slow. The key in

minimizing this error is to fly low enough to reduce the pixel size (1 m or less) yet to cover the complete area of view desired (i.e., the experimental fire area).

The use of relatively simple infrared technology to monitor fires allowed a detailed characterization of the spatial and the temporal movement of the fire across the experimental plots (Fig. 3). Given the high resolution data obtained for most of the fires in this study (1x1-m pixels), the information we obtained is far superior to that from more conventional monitoring using timers or dataloggers tied to a coarse sampling grid system, which can only give average spread rates over relatively large areas. Hence, the noticeable difference between the two techniques is the large sample size of rate-of spread values obtained from this infrared approach compared to the one value generally reported in past results (Alexander et al. 1991; Stocks 1987, 1989). For our experimental fires, the initial sample size ranged from 5082 to 21 406 values dependent upon the camera altitude (affecting pixel size) and burned area (Table 3). These large sample sizes for rate of spread provide extremely valuable information for analyzing fire behaviour and fire effects.

The large sample size allowed us both to do detailed spatial analyses and to analyze the reliability of the average (plot-level) rate-of-spread values (Table 3-5). The 99% level of confidence for average rate of spread for our fires (Table 5) ranged from ± 0.07 - 0.54 m/min around the mean. Our analysis showed that we could improve our estimates of spread by removing edge effect (Table 4) and by removing erroneously large rate-of-spread values by assuming the distribution was normally distributed and using only those values within 2 standard deviations of the mean (i.e., 95% of the values) as shown in Table 5. The range of fire-spread values possible can be clearly shown (Fig. 4) to give a clear understanding of the inherent

variability that occurs in the rate of spread during any fire. Figure 4 illustrates what occurred when values were eliminated. The biggest reduction of values occurred when the 10-m perimeter was removed for possible edge effects (Fig. 4b). The only difference between Figures 4b and 4c (where values greater than 2 standard deviations were removed) was the drastic reduction of high values in the composite rate-of-spread class of 30 m/min and greater. Figure 4c probably shows a realistic range of equilibrium spread rates for the burning conditions of this particular fire. However, some of the high values eliminated may represent true spread rates where special fire behavior phenomena have occurred, such as junction zones. These can be isolated out by the techniques described in this elsewhere in this paper and analyzed. The future use of infrared analysis, coupled with better data on the factors that affect rate of spread (e.g., wind speed and direction, fuel types, slope, aspect, etc.), could substantially improve understanding and modelling of fire spread dynamics. If individual images are not composited onto one master image (e.g., Fig. 3) but animated, a video can be produced to visually study and understand the fire spread through the experimental plot.

The rate-of-spread data when combined with fuel consumption data in a GIS analysis can provide a detailed indication of the fireline intensity (Byram 1959) across the plot (Fig. 6). This high-resolution knowledge of fireline intensity (kW/m) will prove useful to fire ecologists in allowing them to relate fire impacts to the actual fire characteristics occurring at the sample point. Areas of interest within the fire can be isolated using GIS filtering capabilities to better understand the relationships between fire behavior and fire effects. Previous approaches related to fire effects research have often assumed that fire behavior was constant over entire study plots. Our data (Figures 3 and 6) illustrate that this assumption is unrealistic. For Fire 5, we showed

how different parts of the image could be masked to help in understanding the influence of the living ground cover on fire spread. The lower than normal sample size for Fire 4 in Tables 4 and 5 is a result of only a small portion of the fire being analyzed. The reason for this was that a point-source fire was ignited and studied prior to the line ignition of the entire plot and a substantial area in one corner of the plot was unburnable due to sphagnum (*Sphagnum* sp.) ground cover. Given the heterogeneous nature of fire behavior and microsites even across small areas, the use of infrared monitoring should help immensely in understanding and modelling fire effects better.

Conclusion

This paper discusses use of aerial infrared digital imagery for detailed documentation , monitoring, and analysis of fire behavior. The temporal and spatial resolution is superior to ground-based measurements that rely usually on course grid sampling patterns. The results obtained are consistent and standardized using the developed analysis software. This minimizes observer bias that can occur in point-based observations estimated on the ground. The high resolution that can be attained allows the inherent variability of fire spread and fireline intensity to be better characterized and to be linked with other spatial data on fire effects, fuel conditions, and other factors. The large database allows statistical analysis to be completed for each fire. Using GIS analysis, various fire behavior parameters can be easily overlaid with other information (e.g., wind field data, fuel loading, fire effect data, etc.) to help develop better models for predicting fire behaviour and fire effects.

Acknowledgement

The authors gratefully acknowledge financial support for this research from the National Aeronautics and Space Administration (NASA) Land Cover Land Use Change (LCLUC) Science Program; the United States Civilian Research and Development Foundation (CRDF) for the Independent States of the former Soviet Union; the Russian Fund of Fundamental Investigation; the United States Department of Agriculture, Forest Service; Natural Resources Canada, Canadian Forest Service; and the Russian Academy of Sciences, Siberian Branch. The continued cooperation and logistical support of the Russian Aerial Forest Protection Service (Avialesookhrana) and Russian Forest Service (Regional and Local Forestry Committees) is greatly appreciated.

References

Alexander, M.E. 1982. Calculating and interpreting forest fire intensities. Can. J. Bot. **60:** 349-357.

Alexander, M.E., B.J. Stocks and B.D. Lawson. 1991. Fire behavior in black spruce-lichen woodland: the Porter Lake project. For. Can., Northern For. Cent. Inf. Rep. NOR-X-310.

Anuchin, N.P. 1982. (5^{th} ed.) Forest Inventory (in Russian). For. Industry, Moscow, Russia.

Belov, S. V. 1976. Forest Pyrology (in Russian). Leningrad For. Acad. of the USSR, St. Petersburg, Russia.

Blank, R.W. and A.J. Simard. 1983. An electronic timer for measuring spread rates of wildland fires. USDA For. Ser. Res. Note NC-304.

Byram, G.M. 1959. Combustion of forest fuels. *In* Forest Fire: Control and Use. McGraw-Hill, New York, NY. pp. 61-89.

Canadian Forestry Service. 1987. Tables for the Canadian Forest Fire Weather Index System. Canadian Forest Service, Forest Technical Report No. 25 (4th edition). Ottawa, ON.

Eenigenburg, J.E. 1983. User's Guide to Calculating Rate of Fire Spread by Hand-held Calculator, USDA For. Serv. Gen. Tech. Rep. NC-89.

Eenigenberg, J.E. 1987. Computer program for calculating and plotting fire direction and rate of spread. USDA For. Serv. Tech. Rep. NC-117.

Forestry Canada Fire Danger Group. 1992. Development and structure of the Canadian Forest Fire Behavior Prediction System. For. Can. Info. Rep. ST-X-3.

Furyaev, V.V. 1996. Fire Ecology of Siberian Boreal Forests. *In* Fire in Ecosystems of Boreal Eurasia, Kluwer Academic Publishers, Netherlands. pp. 168-185.

Korovin, G. N. 1996. Analysis of the Distribution of Forest Fires in Russia. *In* Fire in Ecosystems of Boreal Eurasia, Kluwer Academic Publishers, Netherlands. pp. 112-128.

McRae, D.J., Stocks, B.J., and Ogilvie, C. J. 1989. Fire acceleration on large-scale convection columns. *In* Proceedings of the 10th Conference on Fire and Forest Meteorology, 17-21 April 1989, Ottawa, Ont. *Edited by* D.C. MacIver, H. Auld, and R. Whitewood. For. Can., Chalk River, ON. pp. 101-107.

McRae, D.J. 1996. Prescribed fire aerial ignition strategies. Can. For. Serv., Great Lakes For. Cent. Northern Ontario Development Agreement, Tech. Rep. TR-33.

McRae, D.J. and Jin, J.Z. 2004. An infrared approach to forest fire behavior quantification. *In* Proceedings of the 21st Tall Timbers Conference, 15-18 October 2001, Kananaskis, Alberta *Edited by* R.T. Engstrom, K.E.M. Galley, and W.J. de Groot. Tall Timbers Res. Sta., Tallahassee, FL. pp. 154-162.

McRae, D.J., S.G. Conard, G.A. Ivanova, A.I. Sukhinin, W.M. Hao, K.P. Koutzenogij, S.P. Baker, V.A. Ivanov, Y.N. Samsonov, T.V. Churkina, A.V. Ivanov, and T.W. Blake. 2004. Fire regimes, variability in fire behavior, and fire effects on combustion and chemical and carbon emissions in Scotch Pine forests of central Siberia. Mitigation and Adaptation Strategies for Global Change, Kluwer Academic Publishers, Dordrecht, Netherlands. In press.

Parmuzin, Y.P. 1985. Taiga of the USSR (in Russian), Mysl, Moscow, Russia.

Simard, A.J., Eenigenburg, J.E., Adams, K.B., Nissen Jr., R.L. and Deacon, A.G. 1984. A general procedure for sampling and analyzing wildland fire spread. For. Sci. **30**: 51-64.

Stocks, B.J. 1987. Fire behavior in immature jack pine. Can. J. For. Res. **17**: 80-86.

Stocks, B.J. 1989. Fire behavior in mature jack pine, Can. J. For. Res. 19: 783-790.

Taylor, S.W., B.M. Wotton, M.E. Alexander, and G. N. Dalrymple. 2004. Variation in wind and crown fire behavior in a northern jack pine- black spruce forest. Can. J. For. Res. **34**: 1561-1576.

Valendik, E.N. 1990. Large Forest Fire Control (in Russian), Nauka Publ., Novosibirsk, Russia.

Valendik, E.N and Ivanova, G.A. 1996. Extreme Fire Seasons in the Forests of Middle Siberia. *For*. **4**: 38-42.

Van Wagner, C.E. 1973. Height of crown scorch in forest fires. Can. J. For. Res. **3**: 373-378.

Van Wagner, C.E. 1987. Development and structure of the Canadian Forest Fire Weather Index. Can. For. Serv., For. Tech. Rep. No. 35.

Vonsky S.M., Zhdanko, V.A., Korbut, V.I., Semenov, M.M., Tetjusheva, L.V. and Zavgorodhaja, L.S. 1975. Compiling and Using the Local Scales of Fire Danger in the Forest (in Russian), LenNIILH, Leningrad, Russia.

Table 1. Ambient fire weather parameters, Russian Fire Danger System, and Canadian Forest Fire Weather Index (FWI) System

		Weather parameters*				Russian Fire Danger System		Canadian Forest Fire Weather Index (FWI) System components‡					
Fire No.	Date (dd/mm/yyyy)	Temperature (°C)	Relative humidity (%)	Wind (km/h)	Rain (mm)	Nesterov Index†	Moisture Index†	FFMC	DMC	DC	BUI	ISI	FWI
Yartsevo site													
1	30/07/2002	27.6	50	1.8	0.0	661	1 340	87.7	28.5	285	45.6	3.2	8.7
2	18/07/2000	26.4	21	1.0	0.0	2 093	2 421	92.8	50.5	393	76.4	8.5	24.7
3	25/07/2002	20.6	41	9.3	0.0	797	1 576	88.7	29.2	261	45.7	5.7	13.9
4	26/07/2002	23.2	37	1.2	0.0	1 041	1 820	87.6	31.1	269	48.2	3.1	8.7
Govorkova site													
5	18/06/2002	24.3	26	9.9	0.0	1 057	930	91.5	17.5	113	25.2	5.8	10.3
6	19/06/2002	24.2	24	2.0	0.0	1 522	1 396	92.8	22.2	121	30.4	7.0	13.1

component values associated with each experimental fire monitored by infrared by the current study.

* Based on solar noon weather. Rainfall is the amount measured in the previous 24-hr period.

† Information on the Nesterov Index and Moisture Index can be obtained from Nesterov (1949) and Vonsky (1975), respectively.

‡ Abbreviations are: FFMC-Fine Fuel Moisture Code, DMC-Duff Moisture Code, DC-Drought Code, ISI-Initial Spread Index, BUI-Buildup Index, and FWI-Fire Weather Index. Further component definitions of the FWI System may be found in Canadian Forestry Service (1987).

Table 2. Experimental fire behavior characteristics associated with Scotch pine (*Pinus sylvestris*) located on dry sites in central Siberia. Spread rates are equilibrium (steady state) averages for each experimental fire based on in-ground, rate-of spread timer observations.

Fire No.	Type of fire	Total fuel consumption (kg/m^2)	Depth of burn (cm)	Rate of spread (m/min)*	Fireline intensity (kW/m) †
Yartsevo site					
1	Surface	1.42	3.9	1.4	587
2	Surface	3.07	6.4	9.0	9 018
3	Surface	1.36	4.1	5.0	2 200
4	Surface	2.39	6.1	5.2	3 987
Govorkova site					
5	Surface	1.52	4.6	6.5	3 195
6 (crown fire)	Crown	2.69	5.6	26.7	23 824
6 (surface fire)	Surface	2.21	5.6	6.8	4 876

* Rate-of-spread values were obtained only from the rate-of-spread timers (Blandk and Simard 1983). Values represent average equilibrium spread rates across the plot only.

† All low heat of combustion values have been adjusted to account for actual fuel moisture.

Table 3. A comparison of the rate of spread obtained from our infrared monitoring and analysis versus values obtained from conventional on-ground monitoring. This analysis uses all pixel values monitored for each fire. Note how statistical information can now be included to understand the reliability of the estimates.

Fire No.	Conventional rate of spread (m/min)*	Infrared analysis				
		Average rate of spread (m/min)	Standard error	Maximum pixel value	Sample size (No. of pixels)	Pixel size
Yartsevo site						
1	1.4	2.5 ± 3.6[†]	0.03	144.1	14 126	1.40
2	9.0	6.8 ± 16.4	0.23	804.1	5 082	2.50
3	5.0	15.9 ± 40.8	0.31	2 569.0	17 397	1.28
4	5.2	5.0 ± 10.9	0.10	818.3	12 332	1.18
Govorkova site						
5	6.5	8.9 ± 11.9	0.08	991.7	21 406	1.09
6 (crown fire)[‡]	26.7	19.0 ± 9.7[§]	0.17	521.5	13 166	0.99
6 (surface fire)[‡]	6.8	7.7 ± 11.5[§]	0.11	755.2	11 886	0.99

* Conventional rate of spread values (from Table 2) were obtained only from the rate-of-spread timers (Blank and Simard 1983).

[†] Values shown are the average ± one standard deviation.

[‡] Because of obvious differences in fire behavior characteristics, analysis of Fire 6 was delineated as to what burned as a crown and as a surface fire.

[§] The average rate-of-spread value for the entire image or fire area of Fire 6 was 12.6 m/min.

Table 4. A comparison of the rate of spread obtained from our infrared monitoring and analysis where a 10-m-perimeter section was removed from the analysis to eliminate any possible edge effects (compare these results to values found in Table 3).

Fire No.	Conventional rate of spread (m/min)*	Infrared analysis				
		Average rate of spread (m/min)	Standard error	Maximum pixel value	Sample size (No. of pixels)	Pixel size
Yartsevo site						
1	1.4	2.1 ± 2.9[†]	0.03	144.1	9 406	1.40
2	9.0	5.0 ± 3.1	0.04	804.1	4 901	2.50
3	5.0	16.9 ± 46.7	0.52	2 569.2	8 200	1.28
4	5.2	6.9 ± 15.6	0.31	818.3	2 562	1.18
Govorkova site						
5	6.5	9.0 ± 13.3	0.11	991.7	14 064	1.09
6 (crown fire)[‡]	26.7	20.9 ± 16.5[§]	0.20	521.5	10 106	0.99
6 (surface fire)[‡]	6.8	9.0 ± 6.1[§]	0.06	125.8	11 093	0.99

* Conventional rate of spread values (from Table 2) were obtained only from the rate-of-spread timers (Blank and Simard 1983).
[†] Values shown are the average ± one standard deviation.
[‡] Because of obvious differences in fire behavior characteristics, analysis of Fire 6 was delineated as to what burned as a crown and as a surface fire.
[§] The average rate-of-spread value for the entire image or fire area of Fire 6 was 14.2 m/min.

Table 5. A comparison of the rate of spread obtained from our infrared monitoring and analysis where a 10-m-perimeter edge effect has been removed (Table 4) and only values ± 2 standard deviations of the mean have been used in calculating the average rate of spread (compare these results to values found in Table 4).

Fire No.	Conventional rate of spread (m/min)*	Infrared analysis				
		Average rate of spread (m/min)	Standard error	Maximum pixel value	Sample size (No. of pixels)	Pixel size
Yartsevo site						
1	1.4	2.1 ± 1.6[†]	0.02	5.3	8 465	1.40
2	9.0	5.6 ± 4.6	0.07	14.8	4 411	2.50
3	5.0	11.7 ± 14.1	0.16	39.9	7 380	1.28
4	5.2	4.2 ± 4.2	0.09	12.6	2 301	1.18
Govorkova site						
5	6.5	7.9 ± 5.0	0.04	17.9	12 658	1.09
6 (crown fire)[‡]	26.7	16.9 ± 10.0	0.13	37.0	5 672	0.99
6 (surface fire)[‡]	6.8	7.3 ± 5.9	0.06	18.8	11 092	0.99

* Conventional rate of spread values (from Table 2) were obtained only from the rate-of-spread timers (Blank and Simard 1983).
[†] Values shown are the average ± one standard deviation.
[‡] Because of obvious differences in fire behavior characteristics, analysis of Fire 6 was delineated as to what burned as a crown and as a surface fire.

Figure 1. A map of the living ground cover found on the plot burned by Fire 2.

Figure 2. A picture showing a surface fire (Fire 5) of 3195 kW/m burning in a typical Scotch pine dry site of central Siberia.

Figure 3. A composite map showing the firefront location at 1-minute intervals during Fire 5. The color legend indicates the rate-of-spread class for each individual pixel. The red arrow indicates the fire spread direction. The fire area outside of the box was removed as possible edge-effect error in the calculation of equilibrium rates of spread for Table 4.

Figure 4. Histogram charts of Fire 5 showing: (a) the range of rates of spread for the complete data set (21 406 values) of Table 3, (b) the range of rates of spread (Table 4) when the outer 10-m perimeter is eliminated as edge effect (14 064 values), and (c) when edge effect and erroneous high rates of spread within the fire area (Table 5) are eliminated (12 658 values). Note that conventional rate-of spread measurements using timers would have only given an average value of 6.5 m/min (Table 3) with no statistical confidence level place on this.

Figure 5. A composite map showing the firefront location at 1-minute intervals for Fire 2. Note the convex nature of this firefront as a result of the burnout operation on each side that was trying to keep ahead of the main firefront (head) in the center of the plot. The red arrow indicates the fire direction.

Figure 6. A composite map of Fire 5 showing the fireline intensities (kW/m) based on 1 x 1-m pixel sizes showing the spatial resolution now possible using infrared technology. The fire area outside of the box was removed as possible edge-effect error in the calculation of equilibrium rates of spread.

Figure 7. Composite maps of Fire 5 showing the area (red) of flaming combustion and flame depth at two different times during the fire: (a) 15:39:35, and (b) 15:46:44 LST.

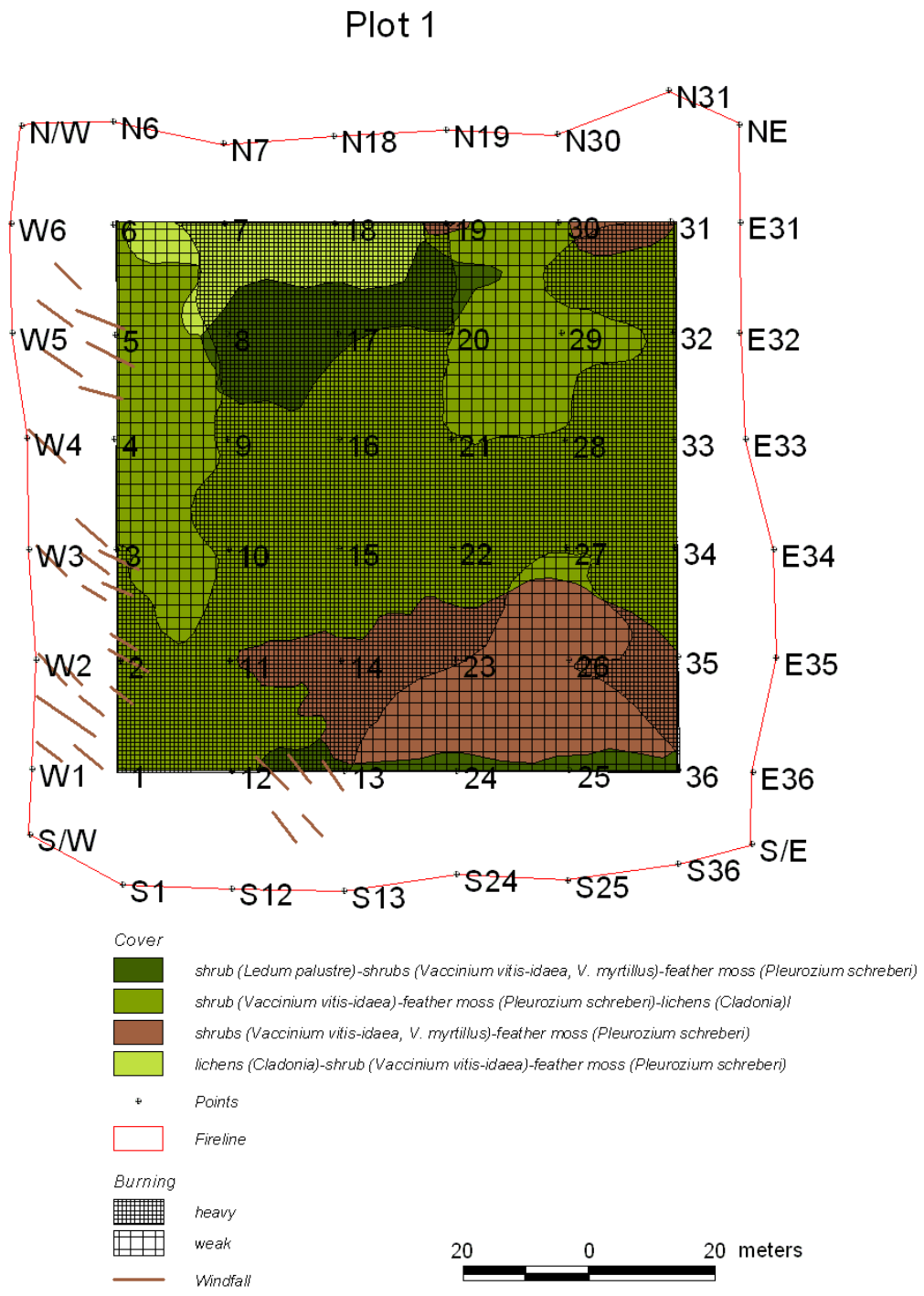
Plot 1
N/W
N6
N7
N18
N19
N30
N31
NE
W6
W5
W4
W3
W2
W1
S/W
S1
S12
S13
S24
S25
S36
S/E
E31
E32
E33
E34
E35
E36
Cover
shrub (Ledum palustre)-shrubs (Vaccinium vitis-idaea, V. myrtillus)-feather moss (Pleurozium schreberi)
shrub (Vaccinium vitis-idaea)-feather moss (Pleurozium schreberi)-lichens (Cladonia)!
shrubs (Vaccinium vitis-idaea, V. myrtillus)-feather moss (Pleurozium schreberi)
lichens (Cladonia)-shrub (Vaccinium vitis-idaea)-feather moss (Pleurozium schreberi)
Points
Fireline
Burning
heavy
weak
Windfall
20 0 20 meters

Figure 1.

Figure 2.

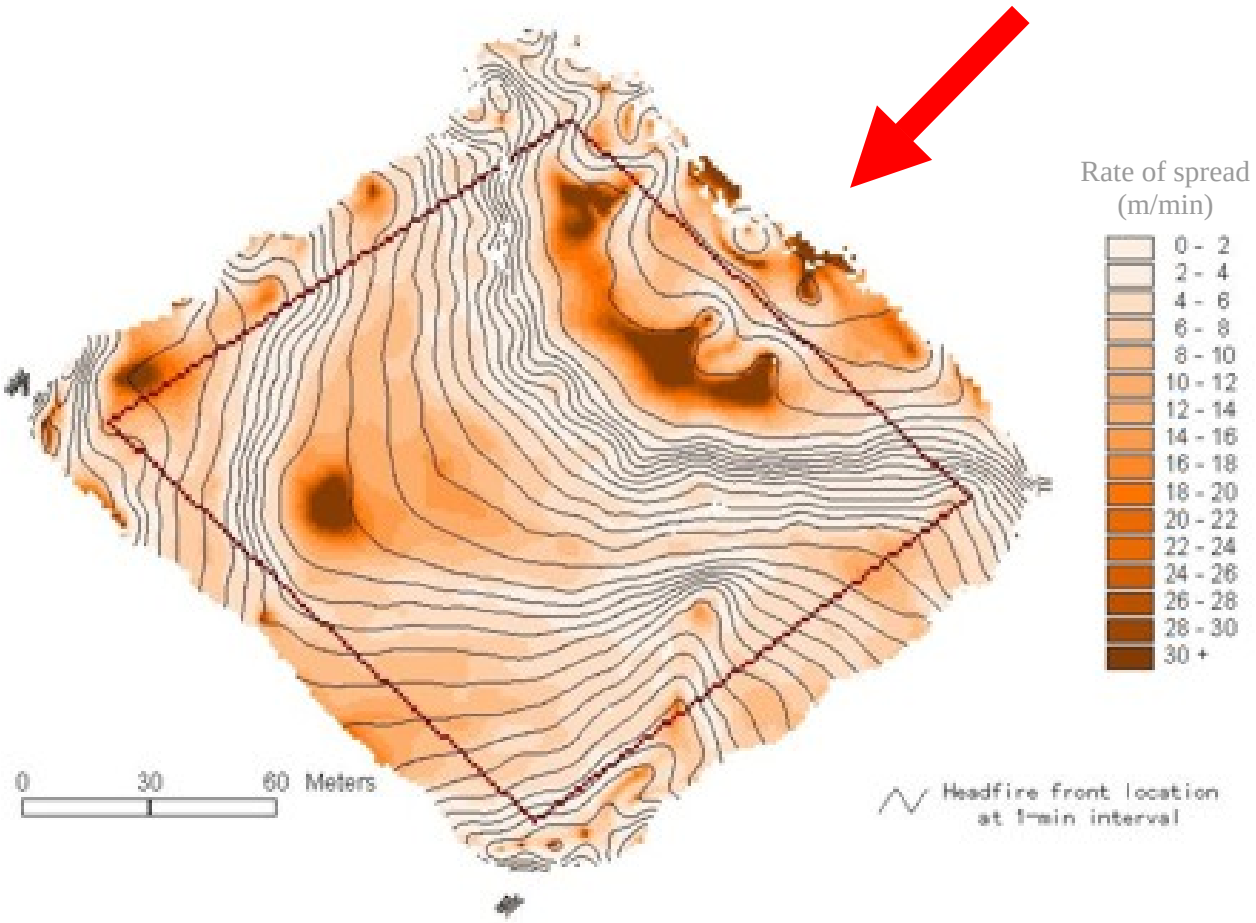
Rate of spread
(m/min)
0 - 2
2 - 4
4 - 6
6 - 8
8 - 10
10 - 12
12 - 14
14 - 16
16 - 18
18 - 20
20 - 22
22 - 24
24 - 26
26 - 28
28 - 30
30 +
0
30
60 Meters
Headfire front location
at 1-min interval

Figure 3.

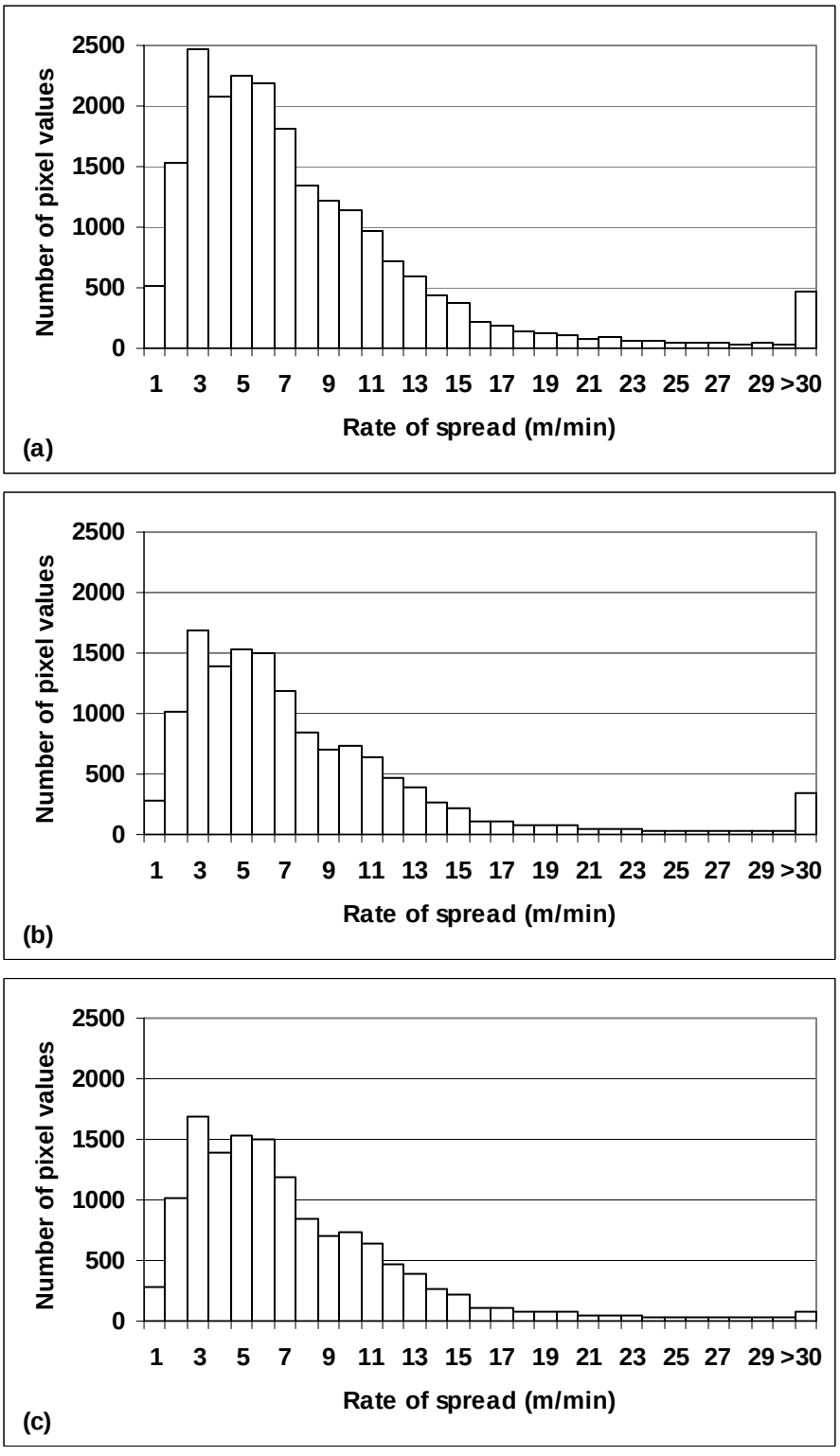
2500
2000
1500
1000
500
0
Number of pixel values
1 3 5 7 9 11 13 15 17 19 21 23 25 27 29 >30
Rate of spread (m/min)
(a)
2500
2000
1500
1000
500
0
Number of pixel values
1 3 5 7 9 11 13 15 17 19 21 23 25 27 29 >30
Rate of spread (m/min)
(b)
2500
2000
1500
1000
500
0
Number of pixel values
1 3 5 7 9 11 13 15 17 19 21 23 25 27 29 >30
Rate of spread (m/min)
(c)

Figure 4.

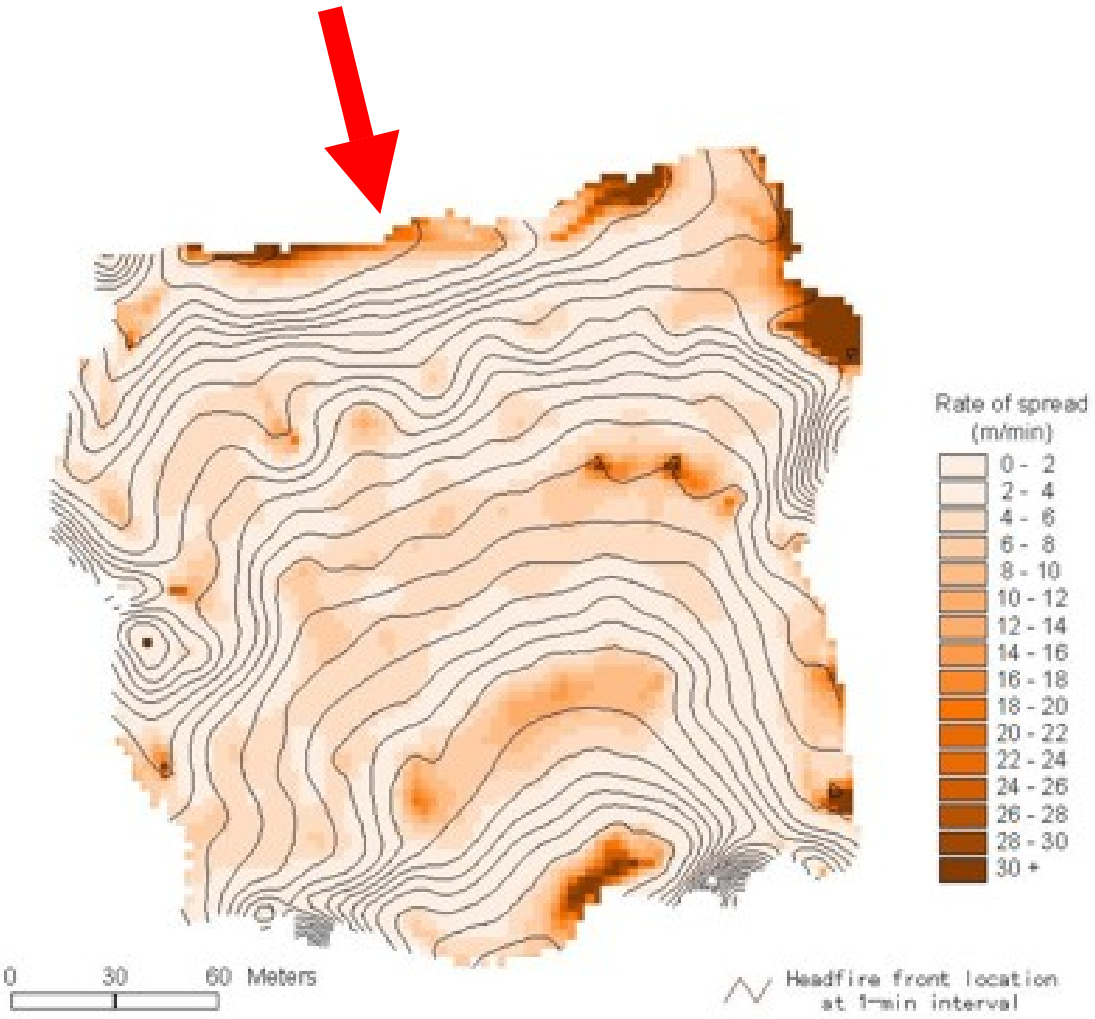
Rate of spread
(m/min)
0 - 2
2 - 4
4 - 6
6 - 8
8 - 10
10 - 12
12 - 14
14 - 16
16 - 18
18 - 20
20 - 22
22 - 24
24 - 26
26 - 28
28 - 30
30 +
0
30
60 Meters
Headfire front location
at 1-min interval

Figure 5.

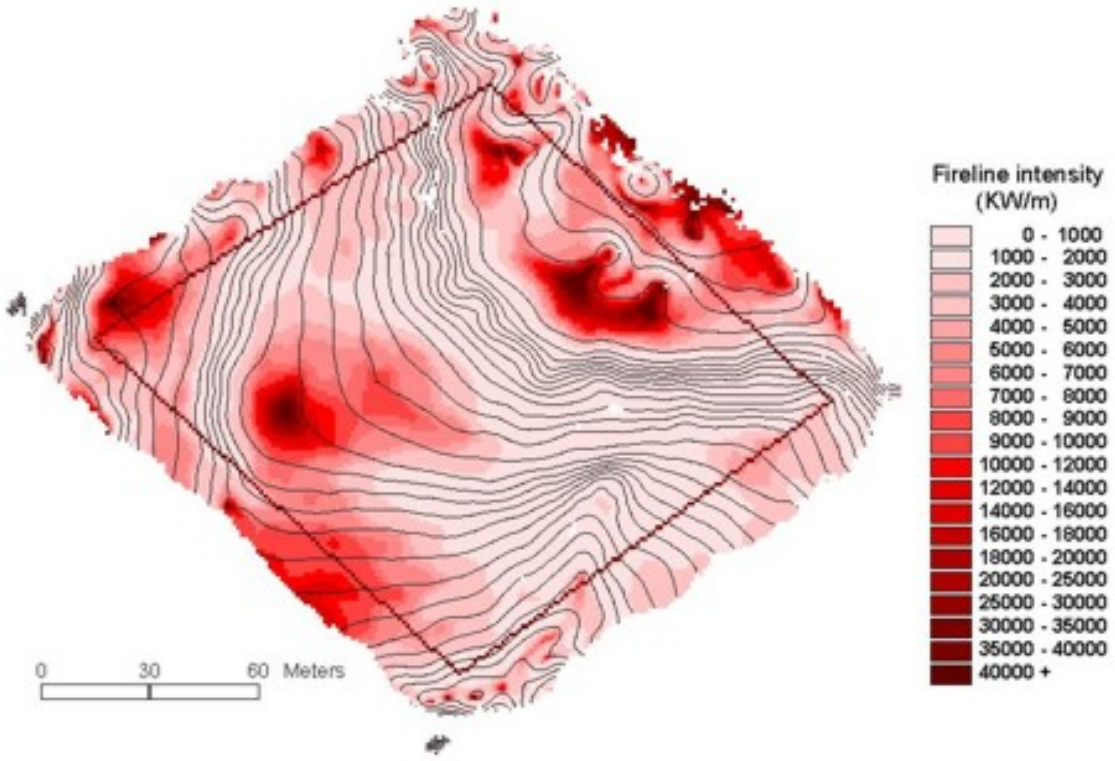
Fireline intensity
(KW/m)
0 - 1000
1000 - 2000
2000 - 3000
3000 - 4000
4000 - 5000
5000 - 6000
6000 - 7000
7000 - 8000
8000 - 9000
9000 - 10000
10000 - 12000
12000 - 14000
14000 - 16000
16000 - 18000
18000 - 20000
20000 - 25000
25000 - 30000
30000 - 35000
35000 - 40000
40000 +
0
30
60 Meters

Figure 6.

(a)

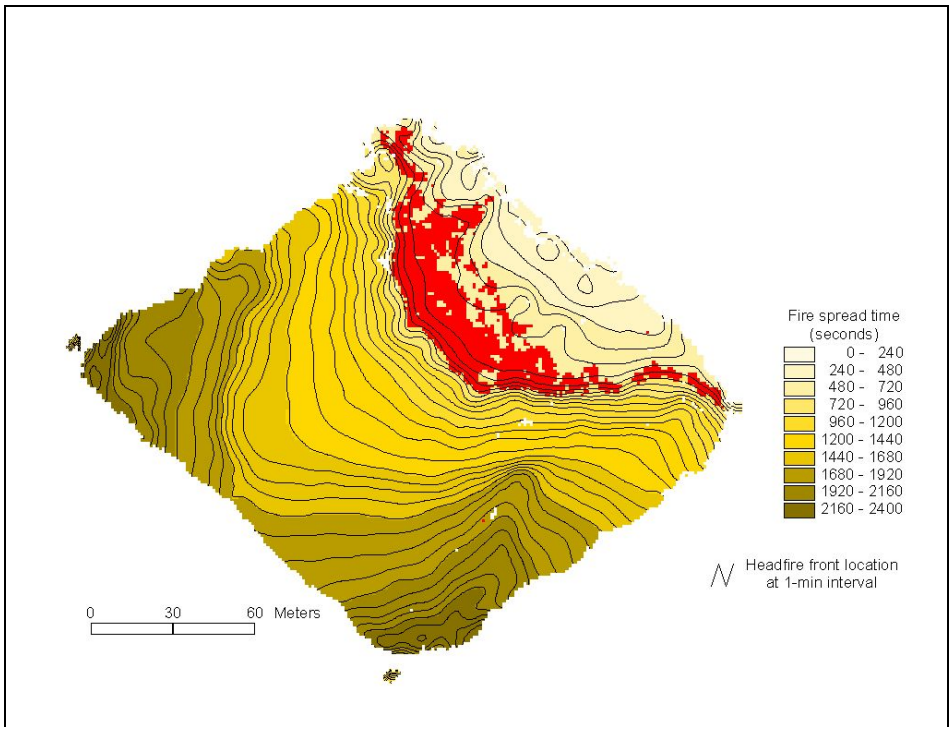
Fire spread time
(seconds)
0 - 240
240 - 480
480 - 720
720 - 960
960 - 1200
1200 - 1440
1440 - 1680
1680 - 1920
1920 - 2160
2160 - 2400
Headfire front location
at 1-min interval
0 30 60 Meters

(b)

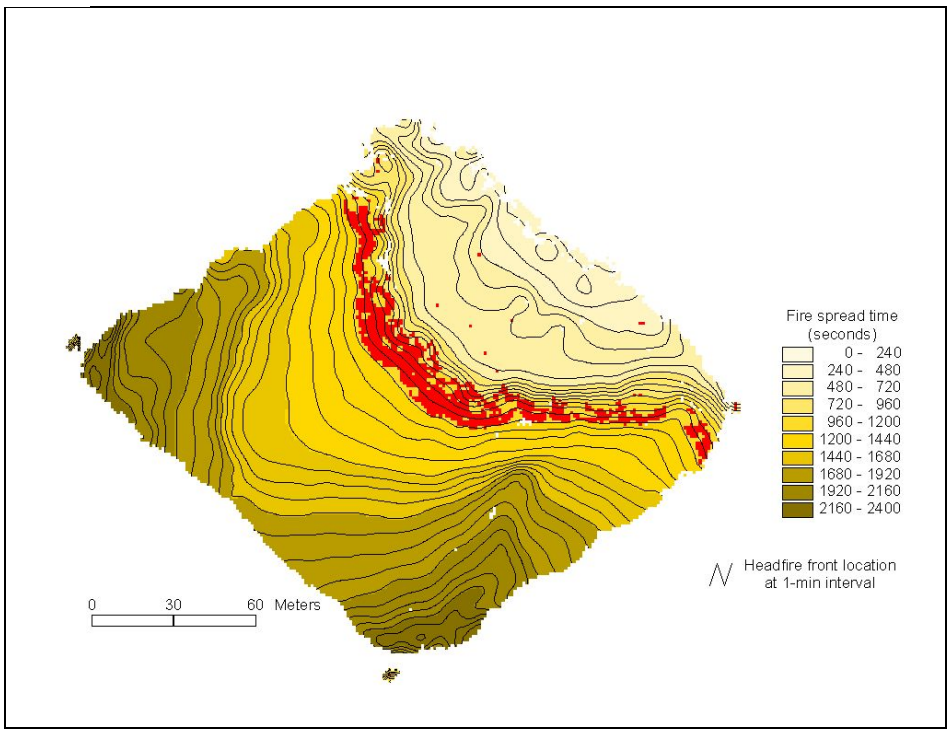
Fire spread time
(seconds)
0 - 240
240 - 480
480 - 720
720 - 960
960 - 1200
1200 - 1440
1440 - 1680
1680 - 1920
1920 - 2160
2160 - 2400
Headfire front location
at 1-min interval
0 30 60 Meters

Figure 7.